JOURNAL OF AIRCRAFT
Vol. 42, No. 6, November–December 2005

Computational Study of F/A-18 E/F Abrupt Wing Stall in the Approach Configuration

Robert J. Niewoehner* and Joshua Filbey†
U.S. Naval Academy, Annapolis, Maryland 21402

This computational study evaluated lateral instabilities observed during developmental testing of the preproduction F/A-18E/F in the power-approach configuration. These instabilities, described here as abrupt wing stall (AWS), occurred whenever the airplane exceeded 12-deg angle of attack. The AWS was quickly corrected in flight test by the closure of a vent at the wing root, without understanding its physical cause or cure. Computational solutions with both the vent open and closed provide insight into the likely cause of the instability, revealing two distinctive flow topologies. Specifically, all F/A-18 Hornet models depend upon strong vortex flows from the leading-edge extension (LEX) to provide lift at elevated angle of attack. Flow through the open vent displaces the LEX vortex core inboard and up off the wing's upper surface. This displacement dramatically weakens the flow stability over the wing's entire upper surface. Wind-tunnel studies performed in parallel by another researcher provide quantitative corroboration of the computational solutions. Finally, computational-fluid-dynamics metrics developed within the NASA/Navy/Industry AWS program are applied to determine their validity at this low-speed flight condition and modified to enhance their viability as predictive tools for AWS prone configurations.

Nomenclature

C_{hprm}	=	sectional contribution to half-plane rolling-moment coefficient
C_l	=	net rolling-moment coefficient (wind tunnel)
$C_{\text{sectional lift}}$	=	sectional lift coefficient in the y direction
c	=	chord
$\bar{c}$	=	mean aerodynamic chord
$2y/b$	=	normalized span distance from plane of symmetry

I. Introduction

THIS project was initiated in spring of 1999 by the Naval Air Systems Command to understand the origin of wing drop on the F/A-18E/F in power-approach (PA) configuration and to provide insight into the mechanism whereby it had been eliminated.

The F/A-18E/F was designed to improve upon the range, payload, growth potential, carrier bring-back, and survivability of the older F/A-18C/D. To this end, the F/A-18E/F design increased the aircraft's dry weight and the wing area by 25%. Preliminary wind-tunnel tests revealed a degradation in the lift generated by baseline leading-edge extension (LEX), leading to an increase of the size of the LEX and an alteration of its shape for the design of the preproduction airplanes. The redesigned LEX started farther aft on the fuselage than on the C/D models and adopted a broader parabolic shape, providing the desired lift.

The increased span of the LEX decreased the leading-edge-flap (LEF) span and significantly affected LEF aerodynamics. A vent in the LEX was created to extend the LEF into the LEX (Fig. 1). Wind-tunnel tests of the LEX vent promised several aerodynamic benefits: 1) increased nose-down pitching moment (providing high angle-of-attack controllability), 2) increased lateral-directional stability, 3) increased maximum lift (cruise/maneuvering configurations), 4) decreased vertical tail buffet (reducing fatigue) at elevated load factor, and 5) increased lift in the PA configuration.

Vent operation was automatic between two positions: fully closed and fully open (33.5 deg leading edge down), opening above 20-deg angle of attack with the gear handle up and whenever the gear handle was down. All landings and catapult takeoffs required the landing gear down, trailing-edge flaps fully deflected to 40 deg, and the leading-edge flaps scheduled with angle of attack (PA configuration).

The first author's initial flight tests of the PA configuration identified a PA wing drop, occurring between 12- and 15-deg angle of attack. Wing drop [now characterized as abrupt wing stall (AWS)] was defined as "an abrupt, uncommanded, roll acceleration," and resulted in a severe degradation in lateral control (level III handling qualities for maintaining wings level ± 5 deg). Super Hornet landings are flown at 8.1-deg angle of attack, sufficiently below the 12-deg AWS onset to avoid a concern on approach. The PA configuration is also used for shipboard catapult takeoffs however, which target 12-deg angle of attack, with expected overshoots to 15 deg. Consequently, the AWS occurred in the heart of the catapult takeoff operating envelope, mandating a corrective engineering effort.

The contractor's wind-tunnel tests, conducted immediately after discovery of the PA-AWS, suggested approximately a dozen candidate configurations for its alleviation, most involving adjustments to the leading- and trailing-edge flap schedules, or the aileron droop. These reflected the suspicion that an outer-wing panel flow problem was responsible for the lift loss. Closure of the LEX vent was deemed the least promising and least attractive candidate—least promising because of the LEX vent's presumed weak effect on the outer wing flow and least attractive because of the predicted value of the LEX vent in lowering the approach speed. (Voicing the consensus skepticism, the project pilot exclaimed during the preflight brief, "Does anybody really imagine closing the LEX vent will work?") Diagnostic flight tests demonstrated that closure of the LEX vent alone eliminated the AWS. Furthermore, contradicting all previous wind-tunnel results, closure of the vent improved the lift and reduced the approach speed.

Solved problems draw little attention. So, in the presence of pressing unsolved problems, the program embraced the fix and pressed ahead. A full study of the PA-AWS was shelved, though neither its physical cause nor its solution were understood. Program managers were relieved that what could have been a vexing problem had been solved so simply and with no adverse collateral effect and pleased to pocket a one-knot reduction in the approach speed.

Presented as Paper 2001-4194 at the AIAA Atmospheric Flight Mechanics, Montreal, Canada, 6–9 August 2001; received 27 July 2004; revision received 3 March 2005; accepted for publication 5 March 2005.

*Capt., USN, Director of Aeronautics, Aerospace Engineering Department, 590 Holloway Road. Member AIAA.

†Lt., USN, Aerospace Engineering Department, 590 Holloway Road.

Fig. 1 F/A-18E in PA configuration with LEX vent open.

The PA-AWS was thereby eliminated by a software patch disabling the LEX vents in the PA configuration, while retaining their use with gear up at high angle of attack. When subsequent testing proved the vents delivered negligible benefit across the flight envelope, they were deleted altogether from the production design, yielding a significant cost, weight, and volume savings.

This study, initiated after the airplane's successful fleet introduction, paralleled two other studies of undesirable lateral behavior. First, a collaborator performed wind-tunnel studies of the identical PA-AWS; his work and its support of this study will be discussed.[1–3] The second was a massive study performed by NASA Langley, the Navy, and Boeing to understand AWS phenomena at transonic speeds applied to a wide range of tactical airplane configurations.[4] The national AWS effort successfully produced a number of candidate diagnostics for predicting AWS behavior in a candidate design, one of which was evaluated for this paper.

II. Computational Procedure, Model and Validation

The computational study utilized the Tetrahedral Unstructured Software System (TetrUSS) because of its assessed suitability for use by an undergraduate researcher.[5] The contractor provided major components of the airplane model, which were then melded together to provide a PA model of the desired fidelity.

The following model simplifications were notable:

1) The trailing-edge flap included no fairings, actuators, brackets, and a fairing over the slot.

2) No landing gear was used.

3) The computational-fluid-dynamics (CFD) model's LEF was fixed at 20 deg down, whereas the airplane's LEF programs automatically with angle of attack.

4) The CFD study used a half-model of the aircraft to limit grid size. The computational model therefore assumed a symmetric airflow employing a reflection plane along the aircraft's plane of symmetry.

5) Time constraints compelled use of an inviscid solution. The validity of modeling highly vortical flows with inviscid computations was substantiated by prior vortex lift research.[6]

Validation of the computational results and justification of the preceding simplifications depended heavily on a parallel wind-tunnel study.[6,7] This work included both 10 and 11.5% models entered in both NASA Langley's 12-foot low speed wind tunnel as well as the Glenn Martin tunnel at University of Maryland. The scope of the tests included a range of angles of attack, sideslip angles, various LEF deflections, and stabilator positions and provided on- and off-body flow visualization as well as force and moment data. These results have been published independently and will be summarized here only insofar as they impacted the computational effort.

The wind-tunnel model geometries lacked both flap hardware (brackets and fairings) and landing gear, replicating these simplifications of the CFD models. Furthermore, wind-tunnel tests performed with the flap slot both open and faired demonstrated that the AWS phenomena was unaffected, thereby justifying this substantial simplification to the high lift geometry.

The wind-tunnel entries provided substantial quantitative data on the total lift variations with angle of attack. Figure 2 presents vent-open and vent-closed lift coefficient results for the configuration closest to the CFD study. (LEF deflection is 10 deg vice 20 deg.

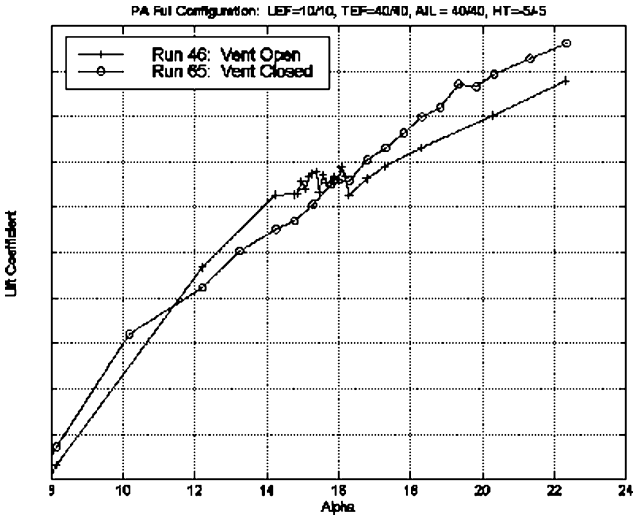

Fig. 2 Wind-lift-coefficient results depicting notch with vent open.

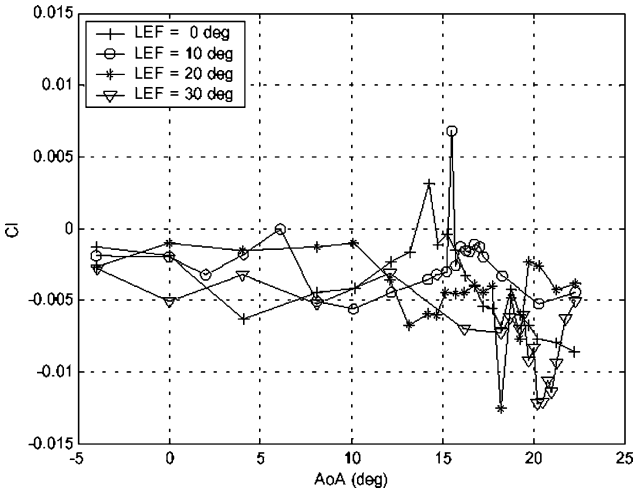

Fig. 3 LEF influence on rolling-moment coefficient.

The ordinate values were removed to protect proprietary data.) Vent closed, the lift curve increases monotonically with increasing angle of attack. The vent-open configuration, however, exhibits a distinct notch in the lift curve between 14- and 17-deg angle of attack. Significantly, erratic dynamic loads on the model and sting through this angle-of-attack range precluded precise definition of the notch, indicative of chaotic, unsteady flow. The notch in the vent-open lift curve and the unsteady loads correlated with spikes in the rolling moment. If CFD results could replicate the notch in the lift-curve slope and a discontinuity in the rolling moment, then they would be regarded as replicating the phenomena and substantiating the grid density, despite the simplified geometry (e.g., faired slot, inviscid, fixed LEF, etc).

Furthermore, wind-tunnel study explored AWS sensitivity to LEF deflections. Four different flap settings were tested vent open, and abrupt asymmetric rolling moments of similar magnitude occurred in each case, the LEF position influencing only the angle of attack at which AWS occurred, and the onset angle of attack increasing markedly with LEF position (Fig. 3). Significantly, this wind-tunnel result did not perfectly correlate with the flight experience, where the AWS occurred at much lower and smaller range of angles of attack. Flight AWS events were in the range 12–14 deg for all LEF settings. Consequently, the fixed LEF setting for the CFD model was considered legitimate, and its exact position immaterial to the behavior we hoped to observe.

Finally, the wind-tunnel studies evaluated the influence of sideslip. Strong asymmetric variations in the rolling moment were

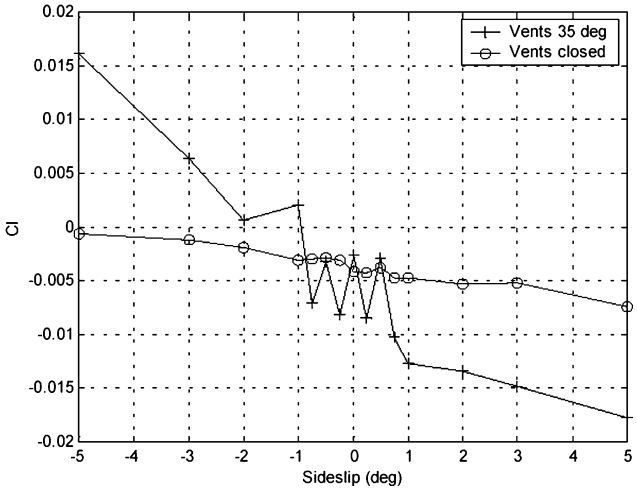

Fig. 4 Rolling-moment variation with sideslip.

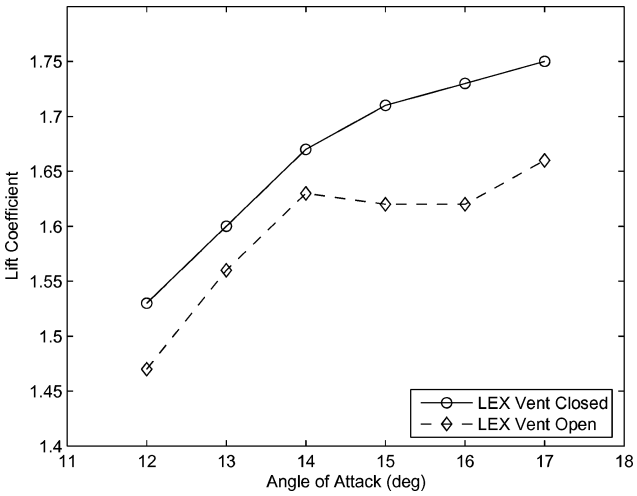

Fig. 5 CFD vent-open/closed lift coefficient results.

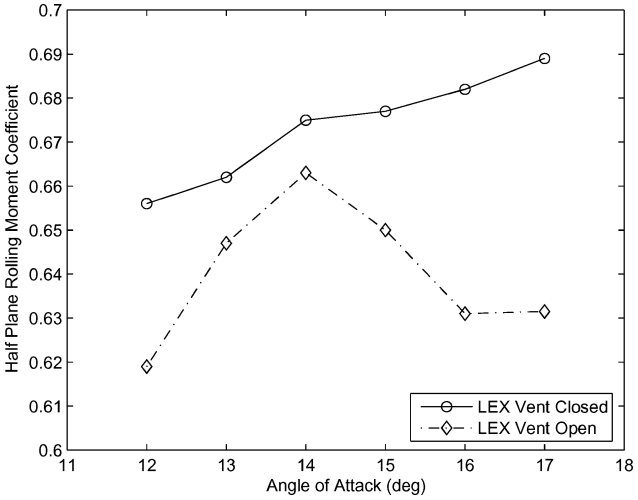

Fig. 6 Half-plane rolling moment.

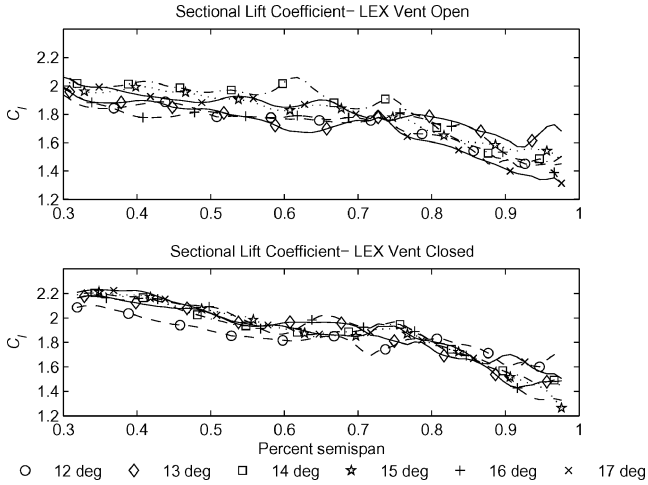

Fig. 7 Sectional lift coefficient.

observed coincident with the vent-open lift-curve notch at a wide range of sideslip angles (Fig. 4). Therefore, because the moment spike was insensitive to sideslip, an asymmetric rolling moment can exist in the presence of a symmetric freestream flow on a symmetric model (zero sideslip), such as was modeled computationally.

III. Results

A. Quantitative Results

Solutions were calculated for both the LEX vent-open configuration and the LEX vent-closed configuration in 1-deg increments from 12- to 17-deg angle of attack. Leading-edge flaps were set to 20 deg, and the stabilator was set to its approximate trim position. A grid of 1.2 million cells was used for the vent-closed configuration, whereas 1.3 million cells were required for the vent-open to capture the geometric details surrounding the vent.

Figure 5 depicts the computed lift curves for the vent-open and vent-closed configurations. Whereas the vent-closed lift increases monotonically throughout the range, the vent-open lift curve drops between 15 and 16 deg. At 16-deg angle of attack, the vent-open lift curve reverses and begins to increase in value again, imitating the wind-tunnel data depicted in Fig. 2. Specifically, the CFD result replicates the 2-deg span over which the tunnel measurements are chaotic, though occurring at an angle of attack more representative of flight than the wind tunnel. The ability of the computational result to replicate this vital feature ("the notch") for both configurations substantiated the simplifying assumptions of the CFD model (e.g., inviscid, fixed LEF, faired TEF slot).

The half-plane rolling moment about the longitudinal axis also shows a strong discontinuity in its variation with angle of attack for the vent-open configuration (Fig. 6). As expected, the rolling moment increases as the lift on the aircraft increases. However, between 14- and 16-deg angle of attack, the vent-open rolling moment decreases sharply. Even though the total aircraft lift only drops by 1% in the notch, the half-plane rolling moment drops by almost 7%! This illustrates how a slight change in lift amplifies to significantly affect the rolling moment and explains how a small loss of lift on one wing is capable of producing a significant unbalanced moment if the lift reduction on the two wings does not occur simultaneously.

An alternate presentation of this data was introduced by the CFD team within the national AWS effort.[7–9] To understand the spanwise variation in the lift, Ref. 7 proposed integrating CFD pressure distributions chordwise, introducing plots of sectional lift coefficients at the range of angle of attack surrounding known AWS behavior. Furthermore, they calculated the local derivative of sectional lift coefficient with angle of attack. AWS-prone configurations were flagged by significant negative deviations in these plots.

For the PA–AWS solutions, sectional lift coefficient and local derivative with angle of attack were determined and depicted in Figs. 7 and 8. A simple forward difference was employed such that the stated derivative at 12 deg is actually the slope of the straight-line segment between the sectional lift coefficient at 12 and 13 deg. The derivatives for this problem are more chaotic than observed for any of the transonic airplanes in Ref. 7, with many span stations exhibiting negative local slopes, albeit with much larger magnitudes (positive and negative) in the case of the vent open.

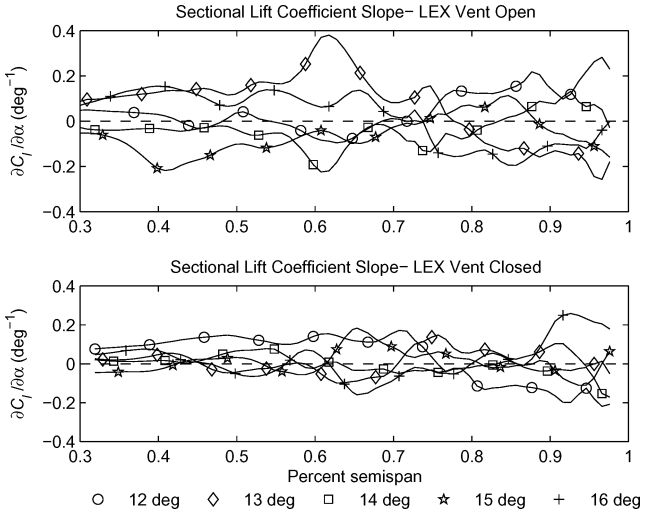

Fig. 8 Sectional-lift-coefficient derivative.

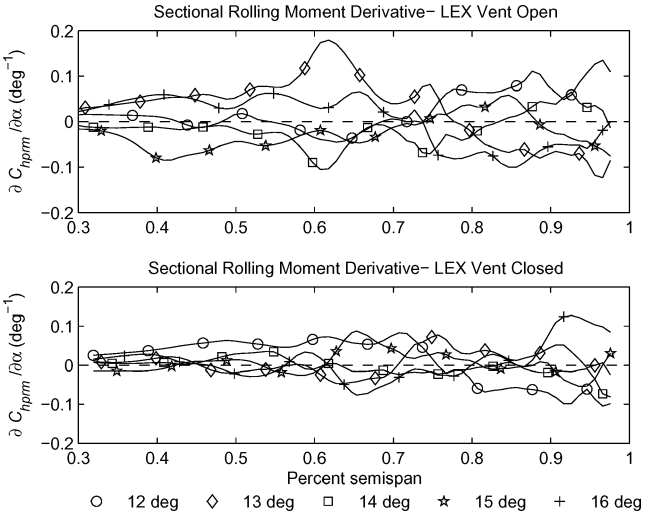

Fig. 10 Sectional-rolling-moment derivative.

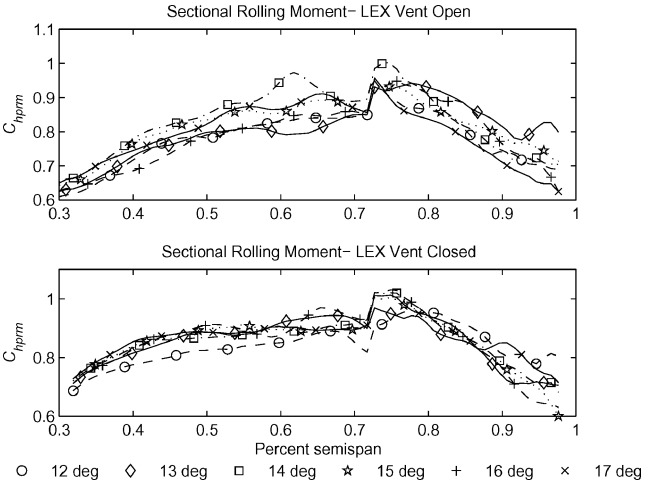

Fig. 9 Sectional-rolling-moment distribution.

To better resolve the rolling-moment contributions, consideration of the sectional lift vs span was extended to the sectional half-plane rolling moment as a function of span location (hprm is used to avoid confusion between subscript l meaning rolling moment or sectional lift).

$$C_{\text{hprm}}\left(\frac{2y}{b}\right) \equiv \left(\frac{2y}{b}\right)^{*}\left(\frac{c}{\bar{c}}\right)^{*}\int_{\text{TE}}^{\text{LE}} \Delta C_p \,\mathrm{d}\left(\frac{x}{c}\right) \qquad (1)$$

This coefficient weights the sectional lift coefficient (the integral) by both the local chord and normalized span location, consequently improving the portrayal of the relative influence of span locations. Figures 9 and 10 depict the spanwise distribution of the sectional rolling-moment contribution and the first derivatives of the rolling-moment contribution with angle of attack. (Note that the discontinuity in the sectional rolling moment at 72% span coincides with the leading-edge snag location and a jump discontinuity in the chord length.) The vent-open moment derivatives have strong unbalanced negative spikes occurring at 62 and 75% span at 14-deg angle of attack. The vent-closed moment derivatives are negative only at higher angle of attack or balanced by compensatory positive values elsewhere along the span.

Two important observations emerge from this presentation format. The first deals with understanding this specific airplane's behavior. Figures 8 and 10 convincingly point to the midspan region as the area in which the vent-open lift loss occurred, provoking the AWS. This agrees with wind-tunnel results that point to the vicinity of the wing surrounding the snag as the area of lift loss.[3] The connection between the vent and the midspan upper-surface flow will be seen more clearly once we examine the off-body flow topologies.

The second observation affirms both the utility and limitations of the sectional slope method of Ref. 7 in flagging AWS-prone aircraft configuration. Reference 7 indicated that the presence of negative derivatives in the spanwise sectional lift distribution indicates an AWS-prone configuration. Furthermore, it reported perfect correlation between AWS configurations and strong negative slopes, whereas some minor negative excursions might be observed for configurations without AWS. In our study, the vent-open AWS configurations exhibit strong negative lift-curve slopes across parts of the span. However, the vent-closed configuration, which demonstrated no AWS susceptibility, also exhibits some negative slopes. There is a marked difference in the magnitudes and character of the two configuration's plots, but as in Ref. 7 a negative slope does not necessarily indicate an AWS-prone configuration. Furthermore, consideration of the sectional-moment contribution in lieu of the sectional lift coefficient portrays the true influence of a span region on any resultant rolling moment. This should be regarded as a minor enhancement of the method proposed in Ref. 7.

The AWS problem can also be described as localized unstable roll damping.[10] The physical mechanism of roll damping is typically described in the following terms: roll rate generates a local increase in angle of attack on the descending wing and an local decrease in angle of attack on the rising wing. Presuming monotonically increasing lift with angle of attack, the descending wing therefore experiences an increase in lift, while the rising wing experiences a decrease in lift; together they create a couple opposing the roll and proportional to roll rate.

By the same rationale, a negative lift-curve slope provides unstable roll damping. The descending wing sees a local angle-of-attack increase, but a decrease in the lift on that wing; the rising wing sees a local angle-of-attack decrease and an increase in lift. Once summed, a propelling rolling moment results. This resembles the classic mechanism for sustained spins, differing in that the upturn in our lift curve slope at 17 deg restores stable roll damping once the local angle of attack on the descending wing exceeds that value.

This latter is very consistent with the first author's personal observations in flight. The wing drops were bounded to small but objectionable angles—bank angle control within 5 deg was impossible (within 1 deg was desired), but no tendency to roll beyond 10 deg was observed. The lift-curve notch should thereby be understood as a localized lateral instability.

Quantitative evaluation of the rolling moment was spawned by consideration of Figs. 9 and 10. A quasi-static roll damping derivative was estimated from the static flowfield solutions by superimposing a linear variation in angle of attack across the span, corresponding to a roll rate of 5 deg/s (representative of the inflight events). The sectional rolling-moment distribution was then determined across

the span by a spline interpolation of the data of Fig. 7. The right wing moment distribution was then subtracted from the left wing and then integrated to generate a rolling moment. The resultant moment was divided by the original roll rate to estimate the roll damping (Fig. 11). The vent-open configuration results in unstable roll damping (a propelling moment, vice damping) at all angles of attack above 14 deg, whereas the vent-closed case indicates unstable damping over only a narrow range. The blended interpolation across multiple flowfield solutions is clearly illegitimate as a true distribution of the forces present in the case of a dynamic rolling maneuver or a numerical evaluation of the roll damping's actual value. The method was attempted solely to discern whether it might appropriately identify tendencies in the roll damping.

An unstable roll damping calculated by this method provides another means by which AWS-susceptible configurations can be flagged. Unfortunately, as with the negative slopes of the sectional lift coefficient, this criterion appears to provide a necessary condition for AWS, but not a sufficient condition. A candidate design exhibiting unstable roll damping, calculated using this method, over a large angle-of-attack range should be suspected to be AWS prone. Likewise, we can conjecture that clearly positive roll damping would be clear of AWS. The method does not unfortunately clear a configuration such as vent-closed, whose calculated roll damping appears slightly unstable, yet is known to not have displayed AWS in flight (Fig. 12).

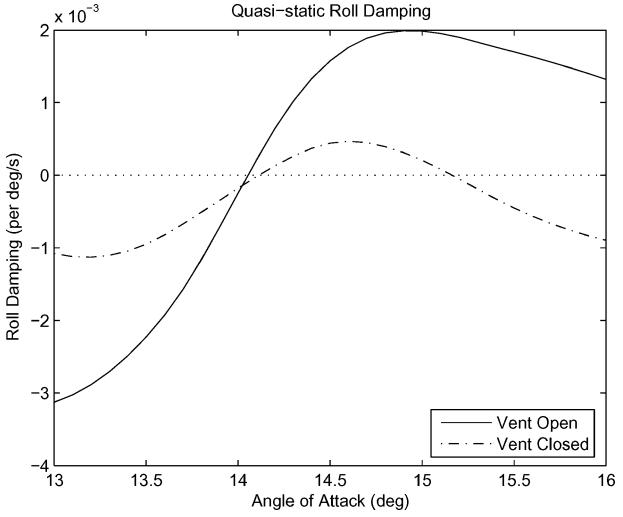

Fig. 11 Quasi-static roll damping.

B. Flow Visualization

Beyond the preceding quantitative results, the question persists, "What feature of the flow caused such drastic differences between the two configurations?" Flow visualizations qualitatively depict the likely cause of the lift loss over the central wing area. These visualizations are best viewed electronically as animation sequences. For the purpose of this paper, however, these are depicted as frames. Each of these visualizations represents both vent-open and vent-closed configurations. Because both configurations used a right-wing model, the solution for the vent-open case was mirrored to produce a left-wing result. This was merged with the right-wing solution for the vent-closed configuration to produce an apparent whole aircraft with one wing in each configuration for side-by-side comparison. The discussion that follows will first consider the on-body, then off-body, flow representations.

1. On-Body Flow Analysis

Considering the pressure distribution on the surface of the aircraft, the vent-open and vent-closed configuration display an obvious difference in their flow patterns. Figure 11 depicts the upper-surface-pressure distributions over the angle-of-attack range from 13 to 16 deg. The left wing portrays the vent-open configuration, whereas the right wing displays the vent-closed configuration. Lower-surface distributions exhibited much more subtle variations and are omitted.

Consider first the 13-deg frame. The outer wing panels exhibit very similar pressure distributions. The inner wings of the two configurations are similar, but do exhibit a distinct difference close to the fuselage, directly aft of the LEX. A strong streak of low pressure runs chordwise aft of the LEX in the vent-closed configuration, indicating the influence of the LEX vortex. In the vent-open configuration, however, that chordwise stream of low pressure does not exist. Conversely, a stream of pressure higher than the surrounding area exists in its place.

This phenomenon becomes more pronounced at higher angle of attack. Recall 14 deg was the angle of attack at which the vent-open lift peaked followed by a lift loss. An obvious disparity now exists between the two central wing areas. The low-pressure stream running aft of the LEX on the vent-closed configuration is much more prominent, influencing the inner and central wing panels. In particular the low-pressure area in the central wing expands monotonically with angle of attack.

The vent-open configuration does not have this pronounced low-pressure stream, with most of the wing at a comparatively high pressure. An intense location of low pressure (suction) does exist at 14 deg, directly aft of the snag, which correlates with the large lift hump depicted at 62% span in Fig. 7. This pocket vanishes in the next frame, correlating with the sign change of the lift coefficient slope in the same location in Fig. 8.

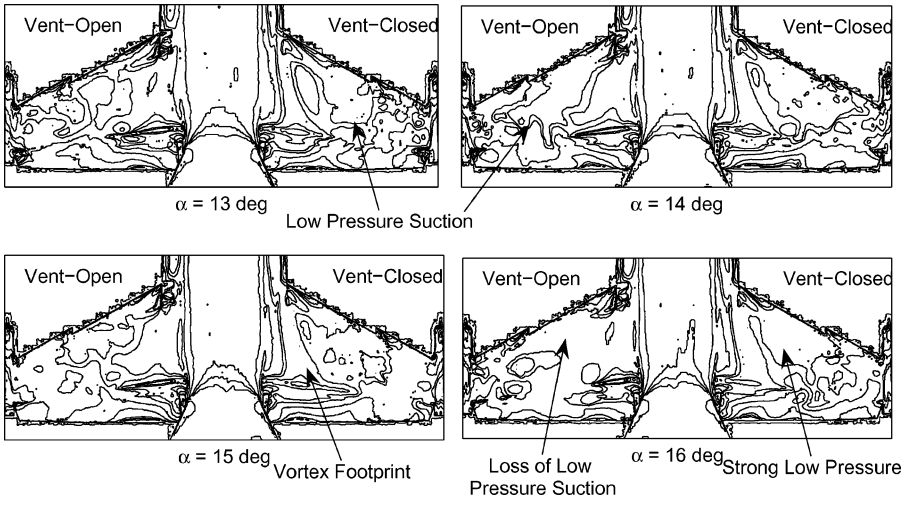

Fig. 12 Upper-surface-pressure distribution.

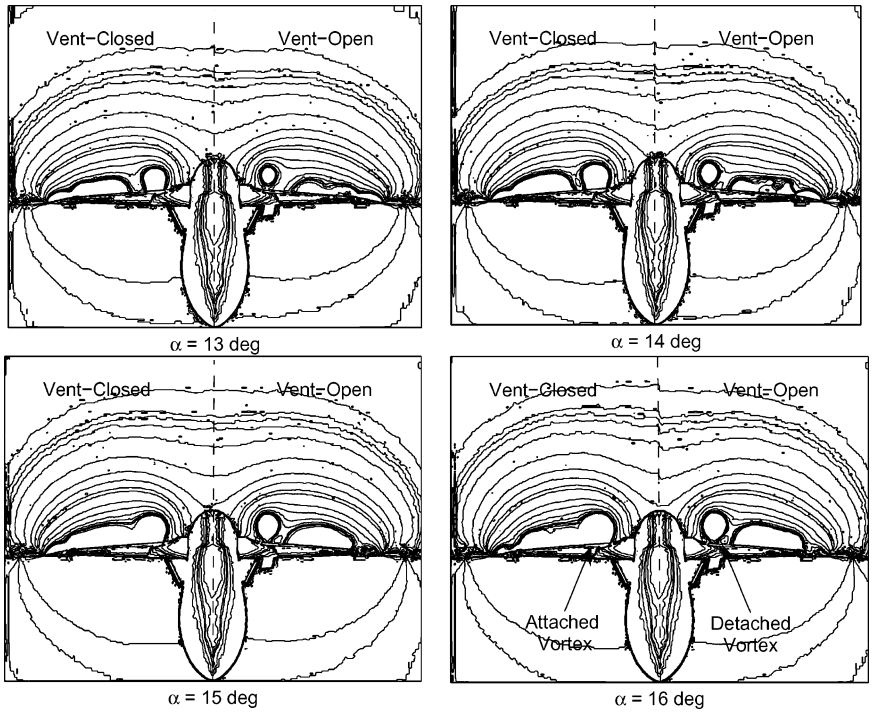

Fig. 13 Off-body pressure map.

Consider the final frame at 16-deg angle of attack. On the vent-closed configuration, the region of low pressure associated with the attached vortex has swollen, correlating with the increased lift previously noted from this wing panel. This region has a large effect on the entire region inboard of the snag, sustaining the flow's attachment. Conversely, the vent-open wing lacks both evidence of an attached vortex or a midspan suction area. Instead, separation spans the central wing region, correlating with the section lift plots already described (Figs. 7 and 8).

2. Off-Body Flow Analysis

The preceding visualizations help to describe the flow along the aircraft's surface. However, in order to fully understand the flow mechanism, the airflow properties off body were also evaluated.

Pressure variance in the *yz* plane (the plane perpendicular to the longitudinal axis) near the quarter-chord provides interesting insight. Figure 13 depicts the aircraft head on at 13- to 16-deg angle-of-attack. The right side of the figure (aircraft's left wing) depicts the vent-open configuration, while the left side of the figure (aircraft's right wing) depicts the vent-closed configuration. The LEX vortex is prominent in all of the frames as the pronounced circular region above the LEX.

The sequence illustrates many summary differences between the vent-open and vent-closed configuration. First, the vortex core is smaller and weaker on the vent-open configuration. It is also detached from the upper wing surface. Furthermore, note that the vent-open vortex is located closer to the airplane centerline. The vent-closed vortex appears centered over the LEX/leading-edge-flap junction, while the vent-open vortex appears centered further inboard.

Considering the pressure distribution at 15-deg angle of attack, both of the vortices are much larger than at 12 deg. The area of low pressure over the wing is much larger, consistent with the increased lift at this angle of attack. Once again, the vent-open vortex is closer to the fuselage centerline and separated vertically from the upper wing surface. It is also distinctly separate from the inner wing's low-pressure bubble, appearing to exert little influence over the central wing lift. In contrast, the central wing bubble on vent-closed configuration merges with the vortex. Thus, the vortex sustains a strong influence over the central wing lift.

Consider the final frame at 16-deg angle of attack, the angle of attack at which the drop in the lift curve was most severe. Vent-open, the low-pressure bubble over the central wing has vanished, attributable for the drop in the lift curve. A large, powerful vortex remains, but vertically displaced from the surface and horizontally isolated from the remnant suction bubble on the inner wing panel. In contrast, vent-closed displays a dramatically different character. The vortex has swollen further and remains attached, directly providing lift while communicating with the low-pressure bubble over the entire central wing, sustaining its attachment.

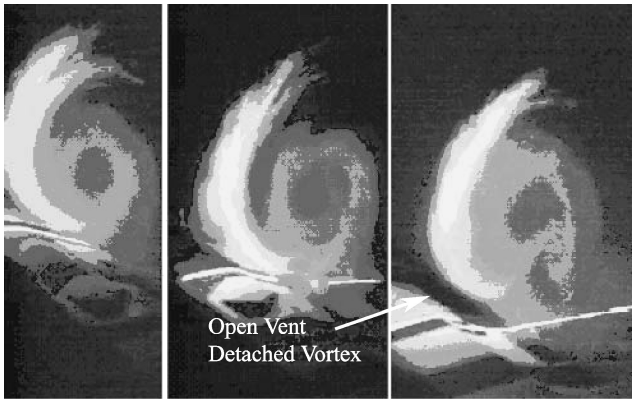

Fig. 14 Vent-open laser sheet of the LEX vortex: forward, above, and aft of vent.

This CFD result provoked the wind-tunnel collaborators to perform a laser-sheet evaluation, depicted in Figs. 14 and 15. The vent-open vortex displacement was measured to be 3.5% up and 1.7% inboard (normalized to the half-span distance), thus confirming the vent's influence on the vortex and the structure of the vortex-midspan interaction.[3]

C. Summary of Results

The lift curve of the vent-open configuration exhibits a characteristic drop between 15- and 16-deg angle of attack. While this lift loss occurs midspan on the wing, it is caused by the displacement of the LEX vortex with the vent open. The vortex of the vent-open configuration is smaller, weaker, detached from the wing surface and closer to the fuselage centerline, decreasing its influence over the lift on the rest of the wing. When the angle of attack of the

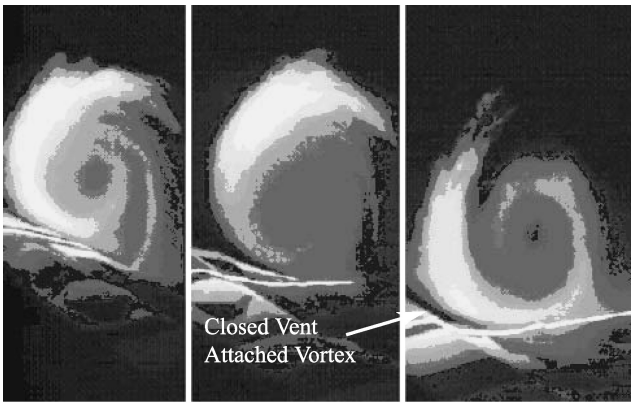

Fig. 15 Vent-closed laser sheet of the LEX vortex: forward, above, and aft of vent.

aircraft increases, the vortex cores grow, as well as the areas of lift over the wing. However, the vent-open lift grows independently of the vortex, whereas the vent-closed lift grows sympathetically with the vortex. At 16-deg angle of attack, the vent-open configuration displays an abrupt decrease in lift, with a consequent reduction in the half-plane rolling moment.

IV. Conclusions

The following significant conclusions can be drawn. First, inviscid CFD identified the flow feature responsible for a major aerodynamic problem in a multibillion dollar development effort, a result affirmed by subsequent wind-tunnel flow visualization. The study highlighted the need for airplane development programs to be sensitive to any breaks in the lift curve, regardless of the flight condition, and points to a means for further evaluating the sensitivity to an AWS behavior. Most importantly, though not formally a part of the national AWS effort, this study confirmed the viability of the CFD methodology proposed in Ref. 7 in flagging AWS-prone configurations. That the flow physics for this problem was radically different than examples considered by the previous work strengthens the case for their method. Finally, the excellent corroboration of inviscid CFD and wind-tunnel results affirmed the conclusion of Ref. 6 that inviscid solvers could adequately model vortex-dominated flows.

Acknowledgments

The work was sponsored by the Naval Air Systems Command (NAVAIR), at the initiative of Jeff Wieringa, then Navy program manager for the F/A-18. Steve Cook (NAVAIR) and Jewel Barlow (University of Maryland) conducted the parallel wind-tunnel study, both efforts shaping and directing the other. Joe Chambers (NASA Langley Research Center) was responsible for educating the entire abrupt-wing-stall (AWS) community that notches in the lift-curve slope for AWS-prone configurations could be recognized as locally unstable roll damping. Finally, Paresh Parikh (NASA Langley) provided considerable direct assistance, both coaching an undergraduate researcher through the computational effort and by postprocessing the results to permit extraction of the sectional lift distribution.

References

[1]Cook, S., and Barlow, J., "Investigation of Effects of Leading Edge Extension Vents on the Lateral Characteristics of the F/A-18 E/F in Power Approach Configuration," AIAA Paper 2000-4510, Aug. 2000.

[2]Cook, S., and Barlow, J., "Investigation of Critical States of the F/A-18 E in Power Approach Configuration Using Mini-Tuft Flow Visualization," AIAA Paper 2001-4145, Aug. 2001.

[3]Cook, S. P., "On Flow Topology Changes Accompanying Aerodynamic Bifurcation for Aircraft with Vented Strakes," Ph.D. Dissertation, Aerospace Engineering Dept., Univ. of Maryland, College Park, MD, March 2003.

[4]Hall, R. M., and Woodson, S. H., "Introduction to the Abrupt Wing Stall Program," *Journal of Aircraft*, Vol. 41, No. 3, 2004, pp. 425–435.

[5]Niewoehner, R. J., and Filbey, J., "Using the TetrUSS CFD Suite in Undergraduate Research," *2000 Proceedings of American Society of Engineering Educators Annual Conference [CD-ROM]*, American Society of Engineering Educators, St. Louis, MO, 2000.

[6]Willams, R. G., "The Computational Investigation of Leading Edge Vortex Breakdown over a Double Delta Wing Configuration," Ph.D. Dissertation, Aerospace Engineering Dept., Univ. of Maryland, College Park, MD, 1999.

[7]Parikh, P., and Chung, J., "Computational Study of the Abrupt-Wing-Stall Characteristics of F/A-18E and F-16C," *Journal of Aircraft*, Vol. 42, No. 3, 2005, pp. 600–605.

[8]Chung, J., and Parikh, P., "A Computational Study of the Abrupt Wing Stall (AWS) Characteristics for Various Fighter Jets: Part II, AV-8B & F/A-18C," AIAA Paper 2003-0747, Jan. 2003.

[9]Woodson, S. H., Green, B. E., Chung, J. J., Grove, D. V., Parikh, P. C., and Forsythe, J. R., "Recommendations for Computational-Fluid-Dynamics Procedures for Predicting Abrupt Wing Stall," *Journal of Aircraft*, Vol. 42, No. 3, 2005, pp. 627–633.

[10]Chambers, J. R., and Hall, R. M., "Historical Review of Uncommanded Lateral-Directional Motions at Transonic Conditions," *Journal of Aircraft*, Vol. 41, No. 3, 2004, pp. 435–447.